Discover Oncology

Analysis

Deciphering the role of acetylation-related gene NAT10 in colon cancer progression and immune evasion: implications for overcoming drug resistance

Xuancheng Zhou[1] · Xun Sang[1] · Lai Jiang[1] · Shengke Zhang[1] · Chenglu Jiang[1] · Yuheng Gu[1] · Yipin Fu[1] · Guanhu Yang[2] · Jieyin Zhang[3] · Hao Chi[1] · Binbin Wang[4] · Xiaolin Zhong[5]

Received: 16 February 2025 / Accepted: 7 May 2025
Published online: 15 May 2025

Abstract

Background Colon cancer (CC) is one of the most common and lethal cancers worldwide, with rising incidence rates in both developed and developing countries. Although advances in treatments such as surgery, chemotherapy, and targeted therapies have been made, prognosis for advanced colon cancer, particularly with metastasis, remains poor. Recent studies highlight the significant role of post-transcriptional modifications like acetylation in cancer biology, affecting processes like gene transcription, metabolism, and tumor progression.

Methods This study applied multi-omics analyses, including single-cell RNA sequencing (scRNA-seq), spatial transcriptomics, and Mendelian randomization. Data were obtained from public datasets like GSE132465, UCSC Xena, and GeneCards. We focused on acetylation-related genes, specifically NAT10 and GNE, using scoring methods, cell–cell interaction models, and survival analyses to investigate their role in colon cancer development, metastasis, and immune evasion.

Results This study identifies that NAT10 is highly expressed in epithelial cells of colorectal cancer (CC) and is closely associated with tumor progression and metastasis. Single-cell RNA sequencing analysis revealed that NAT10-positive epithelial cells exhibited strong interactions with myeloid cells and T cells, with significant differences in cell–cell communication ($p < 0.05$). Based-on-summary-data Mendelian randomization (SMR) analysis further supports a causal relationship between NAT10 and colorectal cancer. In the MR analysis, a significant positive correlation was observed between NAT10 and colorectal cancer risk using summary data from genome-wide association studies (GWAS) and expression quantitative trait loci (eQTL) studies (β_SMR = 0.004, p_SMR = 0.041, p_HEIDI = 0.737). These findings suggest that NAT10 may serve as a pathogenic factor in colorectal cancer development, providing additional genetic evidence that links this acetylation-related gene to colorectal cancer. Survival analysis further demonstrated that NAT10-positive epithelial cells are associated with poorer prognosis. In the TCGA dataset, patients with NAT10-positive epithelial cells exhibited a significantly shorter disease-free survival (DFS) ($p = 0.012$). Unlike GNE-positive cells, NAT10-positive epithelial cells exhibited immune escape characteristics, and TIDE analysis indicated that NAT10-positive epithelial cells were associated with a lower response to immune checkpoint blockade therapy ($p = 1.3e{-}5$), suggesting that they may impair the efficacy of immunotherapy by promoting immune evasion. In contrast, GNE was also significantly expressed in epithelial cells of colorectal cancer, but its role differs from that of NAT10. GNE-positive epithelial cells demonstrated strong communication with immune cells, particularly in interactions between myeloid cells and T cells through receptor-ligand

✉ Hao Chi, chihao7511@163.com; ✉ Binbin Wang, wangbinbinxc@163.com; ✉ Xiaolin Zhong, xiaolinzhong@swmu.edu.cn | [1]Southwest Medical University, Luzhou 646000, China. [2]Department of Specialty Medicine, Ohio University, Athens, OH 45701, USA. [3]First Teaching Hospital of Tianjin University of Traditional Chinese Medicine, Tianjin 300052, China. [4]Intensive Care Unit, Xichong People's Hospital, Nanchong 637200, China. [5]Department of Gastroenterology, Affiliated Hospital, Southwest Medical University, Luzhou 646000, China.

pairs. Despite the important role of GNE-positive epithelial cells in the tumor microenvironment, their association with immune escape is weaker compared to NAT10. Survival analysis revealed that GNE-positive epithelial cells were associated with a better prognosis ($p = 0.015$). In the TCGA dataset, patients with GNE-positive epithelial cells displayed longer disease-free survival (DFS), contrary to the results from the SMR analysis.

Conclusions Leveraging SMR and multi-omics analysis, this study highlights the significant role of acetylation-related genes, particularly NAT10, in colon cancer. The findings suggest that acetylation modifications in epithelial cells contribute to immune evasion and cancer progression. NAT10 could serve as a promising biomarker and therapeutic target for early diagnosis and targeted therapy, offering new avenues for improving colon cancer treatment and patient outcomes.

Keywords Colon cancer · Acetylation · NAT10 · GNE · Single-cell RNA sequencing · Spatial transcriptomics · Immune evasion · Prognosis · Tumor microenvironment · Multi-omics analysis

1 Introduction

Colon cancer (CC) is the third most common malignant tumor worldwide, with high incidence and mortality rates [1]. Known risk factors for colon cancer include genetic susceptibility, dietary habits, obesity, smoking, and chronic intestinal inflammation [2]. The incidence of colon cancer is higher in developed countries, but with the modernization of lifestyle, the incidence has also increased in some developing countries [3]. Colon cancer typically develops from adenomatous polyps into malignant tumors, accompanied by mutations in genes such as APC, KRAS, TP53, and the activation of multiple signaling pathways [4]. Additionally, colon cancer can be classified into right-sided colon cancer (RCC) and left-sided colon cancer (LCC) based on its location, with significant differences in molecular characteristics, clinical manifestations, and prognosis. Right-sided colon cancer is typically associated with larger tumor size, poorer differentiation, and higher rates of distant metastasis, while left-sided colon cancer tends to show better differentiation and lower metastatic potential [5]. The main treatment methods for colon cancer include surgical resection, chemotherapy, radiotherapy, and targeted therapy. Despite continuous advancements in treatment, the therapeutic effect for advanced colon cancer remains limited, especially in patients with distant metastasis [6]. With the in-depth study of the molecular mechanisms of colon cancer, precision medicine and immunotherapy have gradually become new directions for research and treatment strategies [7].

Protein acetylation is one of the important post-transcriptional modifications and is widely involved in various biological processes within the cell, playing a key role especially in gene transcription, signal transduction, and metabolic regulation. The acetylation reaction primarily occurs on the ε-amino group of lysine residues and is catalyzed by lysine acetyltransferases (KATs), while deacetylation is regulated by lysine deacetylases (KDACs) [8]. Acetylation neutralizes the positive charge on the lysine residue, alters the protein conformation, relaxes the chromatin structure, and promotes gene transcription [9]. This modification not only occurs on histones, affecting chromatin structure and gene expression, but also broadly affects non-histone proteins, playing a role in regulating critical biological processes such as the cell cycle, metabolic reprogramming, and protein degradation [10].

In recent years, increasing research has revealed the critical role of acetylation in cancer, particularly in regulating tumor cell proliferation, metastasis, metabolic reprogramming, and drug resistance [11, 12]. In cancer, dysregulated acetylation is closely associated with multiple carcinogenic mechanisms, especially in the silencing of tumor suppressor genes and activation of oncogenes. Studies have shown that alterations in acetylation levels in cancer cells are often correlated with poor clinical prognosis, and mutations in certain acetylation sites may contribute to cancer progression and chemotherapy resistance [13, 14]. In colon cancer research, abnormal regulation of acetylation is closely linked to tumorigenesis and metastasis. For example, the acetyltransferase CBP stabilizes DOT1L through acetylation, thereby promoting the occurrence and metastasis of colon cancer [15]. Meanwhile, the deacetylase HDAC6 deacetylates AKAP12, promoting its ubiquitination and degradation, which enhances the migratory ability of colon cancer tumor cells [16]. Acetylation and deacetylation regulation exerts multiple effects in the occurrence and progression of colon cancer, influencing not only cancer cell metabolism and proliferation but also potentially providing new genetic targets for colon cancer treatment by regulating the expression of key tumor suppressor genes [16, 17]. This study will explore the relationship between acetylation-related genes and colon cancer through multi-omics analysis, revealing the roles of these genes in tumor cell development and metastasis, as well as their impact on the progression of colon cancer.

2 Materials and methods

2.1 Data sources

This study aimed to investigate the characteristics of colon cancer cells and their microenvironment by using the GSE132465 dataset from Sumsang Medical Center. This dataset includes single-cell 3′ RNA sequencing data from 63,689 cells of 23 CC patients, consisting of 23 primary cancer samples and 10 matched normal mucosal samples. The data is available from NCBI (https://www.ncbi.nlm.nih.gov/). In the single-cell scoring analysis, we selected all 33 samples, with subsequent analyses focusing on the 23 primary cancer samples, where tumor samples were analyzed separately, including single-gene expression analysis. Spatial transcriptomics data was provided by 10× Genomics (https://www.10xgenomics.com/). From the HE images, we observed collagen fiber proliferation associated with colon cancer and identified invasive tumor regions with abundant tumor stroma. Additionally, RNA sequencing data for colon cancer was downloaded from the UCSC Xena platform (https://xena.ucsc.edu/), sourced from the TCGA cohort, and used for subsequent survival analysis. The acetylation-related gene set was obtained from GeneCards (https://www.genecards.org/), which contains 11,297 genes.

2.2 Mendelian randomization and summary-data-based Mendelian randomization

Mendelian randomization (MR) is a reliable causal inference method that uses genetic variations as instrumental variables to determine the causal relationship between exposure (such as genes/genomic loci) and outcomes (such as colon cancer) [18]. Instrumental variables are typically single nucleotide polymorphisms (SNPs) that are strongly associated with the exposure ($p < 5e{-}8$), independent of the outcome, and available in both exposure and outcome genome-wide association studies (GWAS). These instrumental variables represent the exposure, and analyzing their effects helps assess whether a causal relationship exists between the exposure and the outcome [19]. Summary data-based Mendelian randomization (SMR) is an advanced method building on traditional Mendelian randomization. It uses summary data from GWAS and expression quantitative trait locus (eQTL) studies to examine pleiotropic associations between gene expression levels and complex traits [20, 21]. In our analysis, we utilized data from the transverse colon and sigmoid colon found in the SMR database, along with colon cancer data from IEU OpenGWAS (https://gwas.mrcieu.ac.uk/), dataset ieu-b-4965 (ncase = 5657, ncontrol = 372,016). We identified 436 genes with strong causal associations to colon cancer ($p\_SMR < 0.05$, $p\_HEIDI > 0.05$) and created the colon cancer SMR gene set.

2.3 Single-cell RNA-seq data analysis

Single-cell RNA-seq data (GSE132465) were downloaded from NCBI, using the cell annotation file provided by the original authors. Dimensionality reduction, clustering, normalization, and visualization were performed. The Seurat package (version 4.4.0) in R (version 4.3.1) was used to extract the gene expression matrix, and five scoring methods (AUCell, Ucells, singscore, GSVA, and addmodulescore) were applied to the colon cancer SMR gene set in the single-cell data to identify cell types highly correlated with colon cancer development. AUCell evaluates whether a gene set is enriched in the top 5% of expressed genes in a single sample by calculating the area under the curve (AUC); UCell calculates the enrichment score of a gene set in a single sample using the Mann–Whitney *U* statistic; singscore computes the enrichment score of a gene set by assessing its deviation from the center; GSVA evaluates the variation of a gene set across samples by performing kernel density estimation of the cumulative distribution function for each gene in each sample; AddModuleScore calculates the average expression of genes in a gene set and compares it with a background gene set to obtain the enrichment score [22–24]. The SMR genes identified through analysis were intersected with the acetylation-related gene set, and genes with a correlation score >10 were identified as colon cancer acetylation feature genes. A new categorical variable, gene_group, was created for each cell based on gene expression, identifying whether cells expressed acetylation-related genes, thus classifying epithelial cells into positive and negative groups. The CellChat package (version 1.6.1) was used to model cell–cell communication interactions and visualize the differences in receptor-ligand pathways between positive and negative cells [25].

Fig. 1 Dimensionality reduction, clustering, colon cancer gene set scoring based on SMR analysis and Mendelian randomization (MR) analysis of the association between acetylation-related genes and colon cancer risk. **A** Principal component analysis (PCA) plot of single-cell data. **B** UMAP and t-SNE visualization of dimensionality-reduced clustered single-cell data, with colors representing different cell clusters (27 clusters in total). **C** UMAP and t-SNE plots for determining cell types. **D** Bar plot of gene expression in cells. **E** Bubble plot showing colon cancer-associated gene scores based on SMR analysis across different cell types in various tissues, using five distinct gene set scoring methods. **F** Violin plot of score differences between cell types under various scoring methods. **G** UMAP plot of colon cancer-associated gene expression in normal and colon cancer tissues based on SMR analysis. **H** Violin plot showing the mean difference in colon cancer-associated gene scores based on SMR analysis across different cell types in various tissues. **I** All available SNPs in the GWAS and eQTL data of NAT10. **J** All available SNPs in the GWAS and eQTL data of GNE. **K** The orange dashed line indicates the effect size estimate of MR associations at top cis-eQTLs, with error bars representing the standard error of the SNP effect

2.4 Pseudotime analysis

Pseudotime analysis is widely used in bioinformatics to study how cells or samples evolve over time or under specific conditions, including in cell development, immune responses, and disease progression [26]. We used the Vector.R code from GitHub to perform UMAP and PCA dimensionality reduction on the single-cell data, mapping high-dimensional data to a low-dimensional space and constructing a grid and network to analyze cell relationships. The code calculates the Quantum Polarization (QP) score to quantify the degree of separation between cell populations, automatically identifying cluster centers and visualizing the relationships and movement directions between cells, thus helping to understand the population structure and dynamic changes of cells.

2.5 Spatial transcriptomics analysis

The Seurat package (version 4.4.0) was used to load and process single-cell data, including data reading, filtering low-quality spots (removing mitochondrial and ribosomal genes), normalization (using SCTransform and LogNormalize), and dimensionality reduction (PCA and UMAP). Then, clustering analysis was performed using the dbscan package (version 1.2-0), with visualization done using ggplot2 and ggpubr, to show the spatial distribution of individual genes on tissue slices [26]. In 10× Genomics Visium technology, each spot is typically 55 μm in size. Given this relatively large size, each spot may encompass multiple cells. The intensity of each spot generally represents the total amount of captured RNA molecules within that area, indicating the expression level of specific genes or the total gene expression in that region.

2.6 RCTD

To bridge the resolution gap between spatial transcriptomics and single-cell omics, the Robust Cell Type Decomposition method (RCTD) was used for deconvolution analysis of each spatial point. The scRNA-seq data was preprocessed strictly, including extracting gene expression matrices, cell annotation information, and total UMI counts per cell. Spatial transcriptomics data was also preprocessed by extracting spatial point location matrices, gene expression matrices, and total UMI counts per spatial point, and RCTD objects were constructed for each tissue slice [27]. The complete RCTD deconvolution pipeline was then run on the RCTD objects to generate cell type weight matrices for each spatial point, and the resulting matrices were normalized so that the sum of cell type weights for each spatial point equals 1. The normalized cell type weight matrices were used to generate proportion matrices, which were integrated and stored in the spatial transcriptomics analysis data for subsequent loading and in-depth analysis.

2.7 MistyR and CellDegree reveal cell communication network

The mistyR package was used to analyze the interactions between cells in three views to reveal the structure of the cell communication network and explore the influence of positive cells in the tumor microenvironment [28]. Subsequently, the CellDegree analysis was performed, where the homotypic cell network describes interactions between similar cell types, while the heterotypic cell network focuses on interactions between different cell types. These networks help analyze the coordination mechanisms within cell populations and the communication between different cell populations, revealing how cells maintain tissue function through signal transmission, and promote or inhibit disease development, especially in the tumor microenvironment and immune responses [29]. Next, a proximity enrichment analysis was performed to investigate the spatial enrichment of T cells and myeloid cells around the positive cells. The number of neighboring T cells

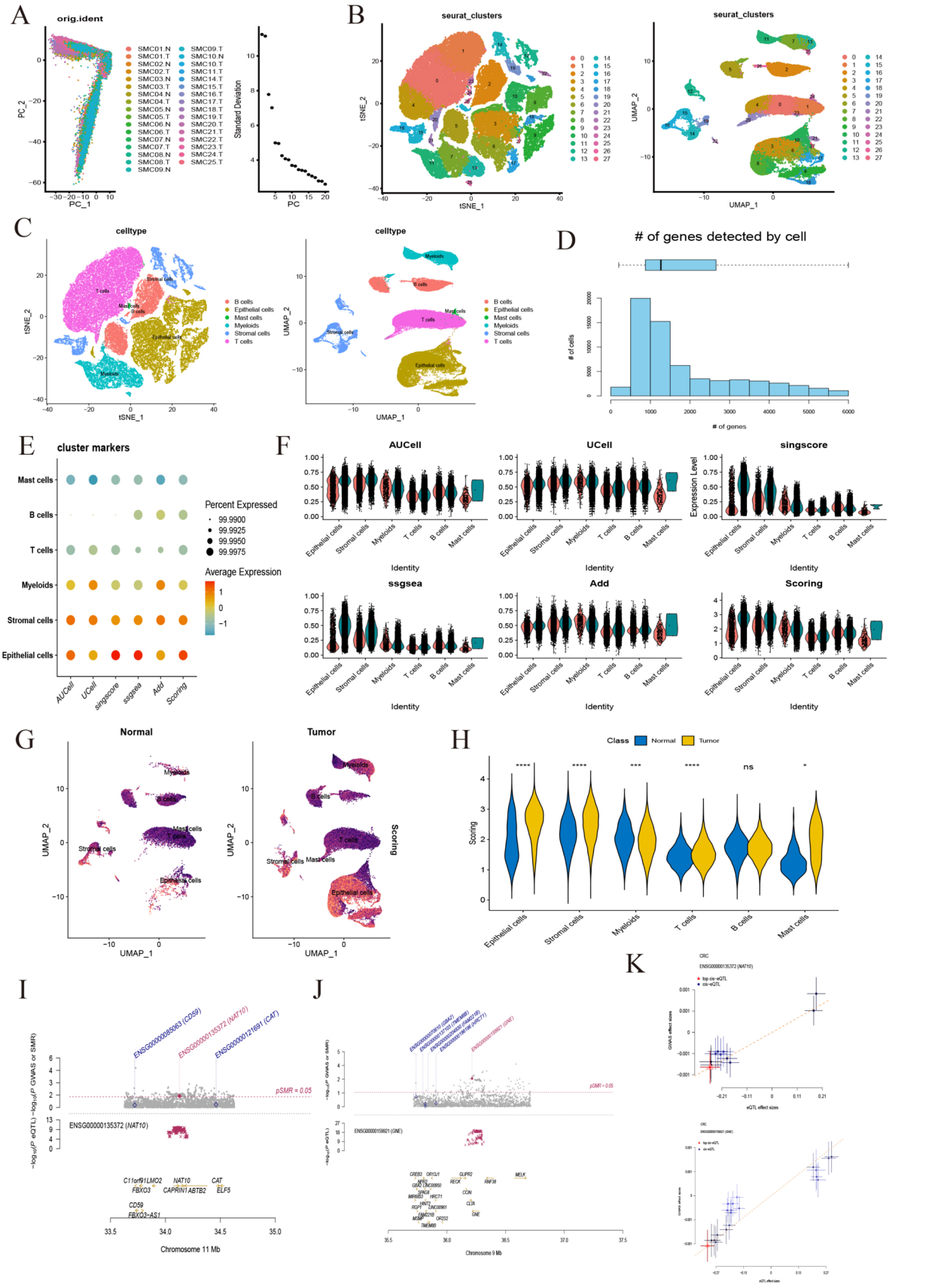
A
orig.ident
PC_2
PC_1
Standard Deviation
PC
B
seurat_clusters
tSNE_2
tSNE_1
UMAP_2
UMAP_1
C
celltype
B cells
Epithelial cells
Mast cells
Myeloids
Stromal cells
T cells
D
# of genes detected by cell
# of cells
# of genes
E
cluster markers
Mast cells
B cells
T cells
Myeloids
Stromal cells
Epithelial cells
AUCell
UCell
singscore
ssgsea
Add
Scoring
Percent Expressed
99.9900
99.9925
99.9950
99.9975
Average Expression
F
AUCell
UCell
singscore
ssgsea
Add
Scoring
Expression Level
Identity
G
Normal
Tumor
H
Class
Normal
Tumor
Scoring
ns
I
ENSG00000085063 (CD59)
ENSG00000135372 (NAT10)
ENSG00000121691 (CAT)
pSMR = 0.05
Chromosome 11 Mb
J
Chromosome 9 Mb
K
CRC
top cis-eQTL
cis-eQTL
eQTL effect sizes

Fig. 2 High and low acetylation level cell communication analysis, pseudotemporal analysis, and spatial probability from the RCTD perspective. **A** Cell communication map of acetylation-related gene set positive epithelial cells, with line thickness representing communication strength. **B** Heatmap of communication strength between different cell types. **C** Receptor-ligand intensity map of signaling pathways between acetylation-positive epithelial cells, acetylation-negative epithelial cells, and T cells. **D** Receptor-ligand intensity map of signaling pathways between acetylation-positive epithelial cells, acetylation-negative epithelial cells, and myeloid cells. **E** Principal component analysis (PCA) plot of epithelial cells. **F** PCA plot of epithelial cells after Harmony integration. **G** UMAP visualization of dimensionality-reduced clustered single-cell epithelial data, with colors representing different cell clusters (13 clusters in total). **H** Intensity map and density plot of acetylation-related gene expression. **I** Pseudotemporal analysis plot of epithelial cells. **J** Spatial distribution probability of various cell types in CC tumor tissue slices analyzed using the RCTD deconvolution method

and myeloid cells was calculated using the K-nearest neighbors (KNN) algorithm, followed by standardized visualization. The results revealed the distribution patterns of different cell types within the tumor microenvironment, providing insights into intercellular interactions and their impact on cancer progression.

2.8 Prognostic analysis

We studied the role of positive epithelial cells in the prognosis of colon cancer. Epithelial cells from tumor samples were selected, grouped based on gene expression, and differentially expressed genes were identified. Bulk analysis was then performed based on TCGA data to evaluate the infiltration of positive cells in tumor tissues. Key genes of positive cells were identified using the FindMarkers function, and GSVA was used to calculate gene set enrichment scores. Survival analysis was conducted using the enrichment scores to assess the correlation between positive cell subgroups and disease-free survival (DFS) in patients. The optimal cut-off value was used to divide patients into high and low expression groups, and survival curves were plotted.

2.9 TIDE

The TIDE (Tumor Immune Dysfunction and Exclusion) database can evaluate the likelihood of tumor escape based on gene expression profiles of tumor samples. The gene expression matrix was standardized and analyzed online using the TIDE database (http://tide.dfci.harvard.edu/), and results were exported. The positive epithelial cell scores were integrated into the results to analyze the relationship between positive cells and immune therapy response. Visual analysis was performed based on TIDE results and the differences between immune responders, as well as correlations with immune cell subgroups, to observe the relationship between various indicators and positive epithelial cells [30, 31].

2.10 Statistical analysis

Statistical analyses were conducted using R 4.2.2 and its associated packages. For continuous variables, the non-parametric Wilcoxon rank-sum test was used to assess relationships between groups. Spearman correlation analysis was used to test correlation coefficients. A significance threshold of $p < 0.05$ was set for all statistical analyses.

3 Result

3.1 Scoring and screening specific cells in the SMR gene set

Single-cell sequencing data, including primary cancer samples (SMC.T, $n = 23$) and matched normal mucosal samples (SMC.N, $n = 10$) (Fig. 1A), were read and normalized. A total of 63,689 cells were clustered into 27 groups and visualized using tSNE and UMAP (Fig. 1B). After cell annotation using the annotation file provided by the original authors, cells were categorized into B cells, Myeloids, T cells, Epithelials, Mast cells, and Stromal cells (Fig. 1C). We selected 436 genes from the SMR analysis for scoring. The distribution of the number of genes detected in each cell was mostly concentrated, while a higher number of genes may indicate greater gene coverage in some cells (Fig. 1D). Various scoring methods (AUCell, UCell, Singscore, ssGSEA, Add, Scoring) revealed differences in expression levels among different cell types (e.g., epithelial cells, stromal cells, myeloid cells), particularly in epithelial cells and myeloid cells, where expression was higher (Fig. 1E, F). The distribution of different cell types in tumor and normal tissues showed a particularly significant

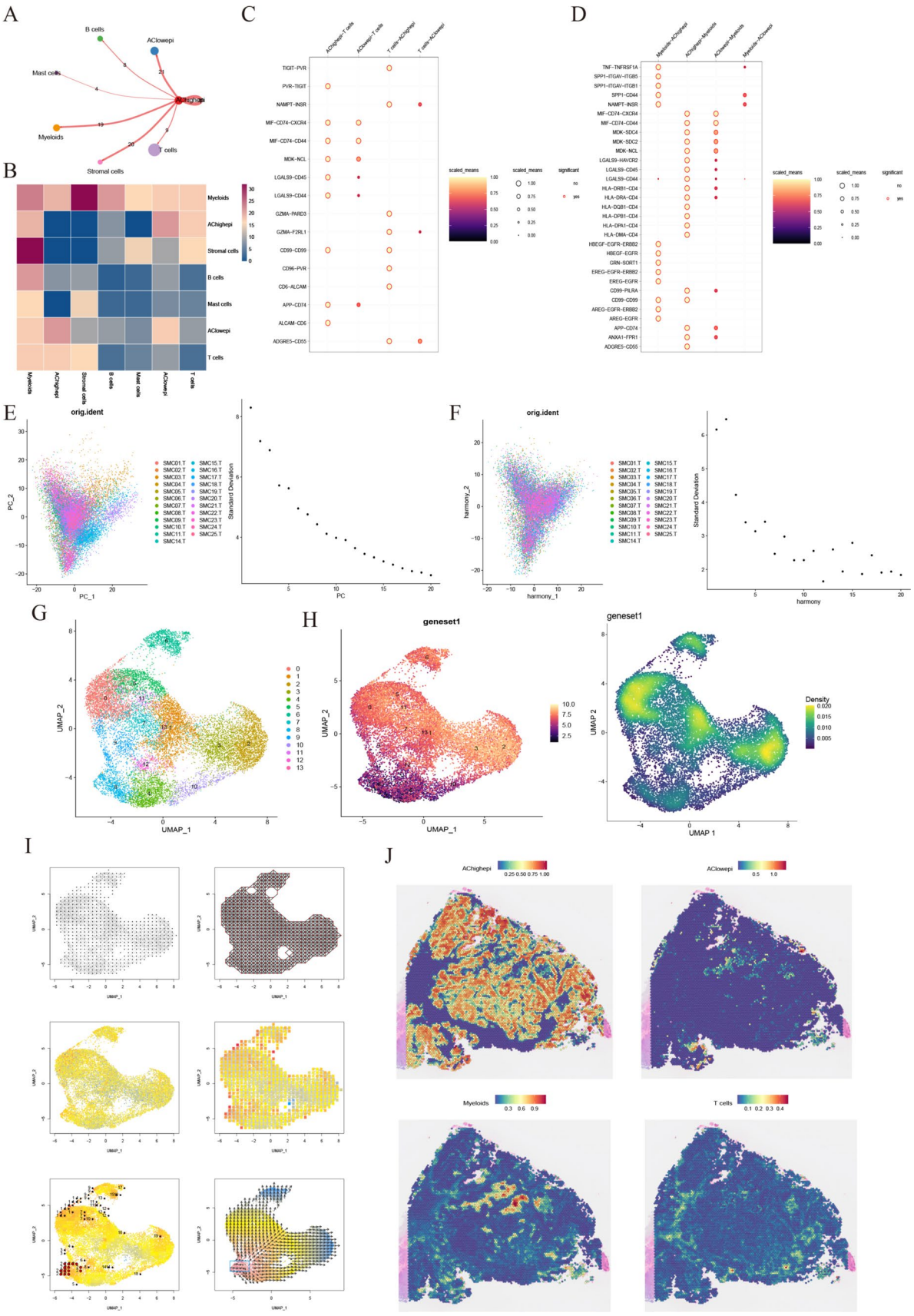
A
B cells
AClowepi
Mast cells
AChighepi
Myeloids
T cells
Stromal cells
B
Myeloids
AChighepi
Stromal cells
B cells
Mast cells
AClowepi
T cells
C
AChighepi-T cells
AClowepi-T cells
T cells-AChighepi
T cells-AClowepi
TIGIT-PVR
PVR-TIGIT
NAMPT-INSR
MIF-CD74-CXCR4
MIF-CD74-CD44
MDK-NCL
LGALS9-CD45
LGALS9-CD44
GZMA-PARD3
GZMA-F2RL1
CD99-CD99
CD96-PVR
CD6-ALCAM
APP-CD74
ALCAM-CD6
ADGRE5-CD55
scaled_means
significant
D
Myeloids-AChighepi
AChighepi-Myeloids
AClowepi-Myeloids
Myeloids-AClowepi
TNF-TNFRSF1A
SPP1-ITGAV-ITGB5
SPP1-ITGAV-ITGB1
SPP1-CD44
NAMPT-INSR
MIF-CD74-CXCR4
MIF-CD74-CD44
MDK-SDC4
MDK-SDC2
MDK-NCL
LGALS9-HAVCR2
LGALS9-CD45
LGALS9-CD44
HLA-DRB1-CD4
HLA-DRA-CD4
HLA-DQB1-CD4
HLA-DPB1-CD4
HLA-DPA1-CD4
HLA-DMA-CD4
HBEGF-EGFR-ERBB2
HBEGF-EGFR
GRN-SORT1
EREG-EGFR-ERBB2
EREG-EGFR
CD99-PILRA
CD99-CD99
AREG-EGFR-ERBB2
AREG-EGFR
APP-CD74
ANXA1-FPR1
ADGRE5-CD55
scaled_means
significant
E
orig.ident
PC_2
PC_1
Standard Deviation
PC
F
orig.ident
harmony_2
harmony_1
Standard Deviation
harmony
G
UMAP_2
UMAP_1
H
geneset1
UMAP_2
UMAP_1
geneset1
UMAP_2
UMAP 1
Density
I
J
AChighepi
AClowepi
Myeloids
T cells

Fig. 3 Cell communication of high acetylation level cells in spatial transcriptomics data. **A** Communication strength of various cell types in the homotypic cell network. **B** Communication strength of high acetylation level cells with myeloid cells (top) and T cells (bottom) in the heterotypic cell network. **C** Enrichment analysis of neighboring cells. **D** Cell interaction relationships from the MistyR perspective. **E** Bar plot showing the contribution of different views to the cell interaction evaluation by the MistyR package, highlighting the relative importance of each. **F** Communication strength and interaction networks of cells under three different perspectives

presence of epithelial cells and gene set expression (Fig. 1G), with epithelial cells also revealing significant differences ("*****") (Fig. 1H). Based on the analysis, epithelial cells were identified as differential cells in colon cancer and will be the focus of subsequent research.

3.2 High expression genes related to acetylation

Due to the large number of acetylation-related genes, and to ensure the efficiency of therapeutic targets, we selected genes with scores greater than 10 from GeneCard and intersected them with the SMR colon cancer genes. Finally, NAT10 and GNE were identified as colon cancer genes highly related to acetylation and were used for multi-omics analysis. Gene localization information has been labeled at the corresponding chromosomal locations, with the related SNPs of NAT10 located on chromosome 11 (Fig. 1I) and GNE located on chromosome 9 (Fig. 1J). Some SNPs of NAT10 (β_SMR = 0.004, p_SMR = 0.041, p_HEIDI = 0.737) and GNE (β_SMR = 0.004, p_SMR = 0.003, p_HEIDI = 0.179) showed significant positive correlations between the GWAS and eQTL effects, indicating that they may be potential risk factors (Fig. 1K).

3.3 Expression of acetylation-related gene set in colon cancer single-cell transcriptomics and spatial transcriptomics

Based on the expression levels of 11,297 acetylation-related genes from GeneCard, epithelial cells were classified into AChighepi and AClowepi. AChighepi exhibited stronger communication with other cell populations, particularly T cells and myeloid cells (Fig. 2A). Differences in communication intensity and frequency were evident, especially in interactions with these immune cells (Fig. 2B). Several ligand-receptor pairs showed strong interactions across multiple cell populations, with AChighepi displaying the most significant interactions. Notably, the TNF-TNFRSF1 pair mediated communication between AChighepi and myeloid cells, potentially influencing immune regulation in the tumor microenvironment (Fig. 2C). For AChighepi and T cells, the most prominent interaction involved the HLA-DRB1-CD4 pair, which may contribute to immune evasion (Fig. 2D). These findings underscore the key role of immune-epithelial cell interactions and acetylation in colon cancer risk. Principal component analysis (PCA) of epithelial cells identified major sources of data variation (Fig. 2E). Batch effect correction using Harmony improved data integration, with recalculated PCA results clarifying cell population distribution (Fig. 2F). An optimal dimensionality reduction parameter (PC = 10) was determined, leading to the identification of 13 distinct clusters (Fig. 2G). Gene expression and density plots highlighted clusters 4, 8, and 10 as having elevated acetylation-related gene expression (Fig. 2H). Cell trajectory analysis with Vector.R revealed that clusters with high acetylation-related gene expression served as the endpoints for dynamic transitions, providing strong evidence for the role of acetylation genes in colon cancer progression (Fig. 2I).

For colon cancer spatial transcriptomics tissue samples and HE staining images, we processed the data by performing dimensionality reduction and clustering of cells, followed by deconvolution analysis using single-cell data to observe the distribution and proportion of AChighepi, AClowepi, myeloid cells (Myeloids), and T cells. The results showed that AChighepi had a wider distribution and higher expression levels (Fig. 2J). After understanding the spatial heterogeneity, we performed CellDegree analysis, where the CellDegree graph displayed the interaction network between cells. Each cell is represented as a node in the network, with connecting lines between nodes indicating interactions or associations. This visualization provides an overall view of the relationships between cell populations and their interactions. The homotypic cell network analysis aimed to construct an interaction network between cells, and certain regions of the AChighepi cell population exhibited higher connectivity, which may indicate that these cells play a key role in the tumor microenvironment, communicating more with immune or stromal cells, with some interactions also occurring between myeloid cells and T cells (Fig. 3A). In the heterotypic cell network, the spatial interaction between myeloid cells and AChighepi was stronger than with T cells (Fig. 3B). Enrichment analysis of neighboring cells further supported this conclusion (Fig. 3C). Based on the deconvolution analysis, misty framework was used to investigate the intercellular relationships in spatial transcriptomics, revealing the interactions and strengths between different cell populations (Fig. 3D). Multi-view modeling was performed using three different spatial context views: intraview, juxtaview, and paraview. The

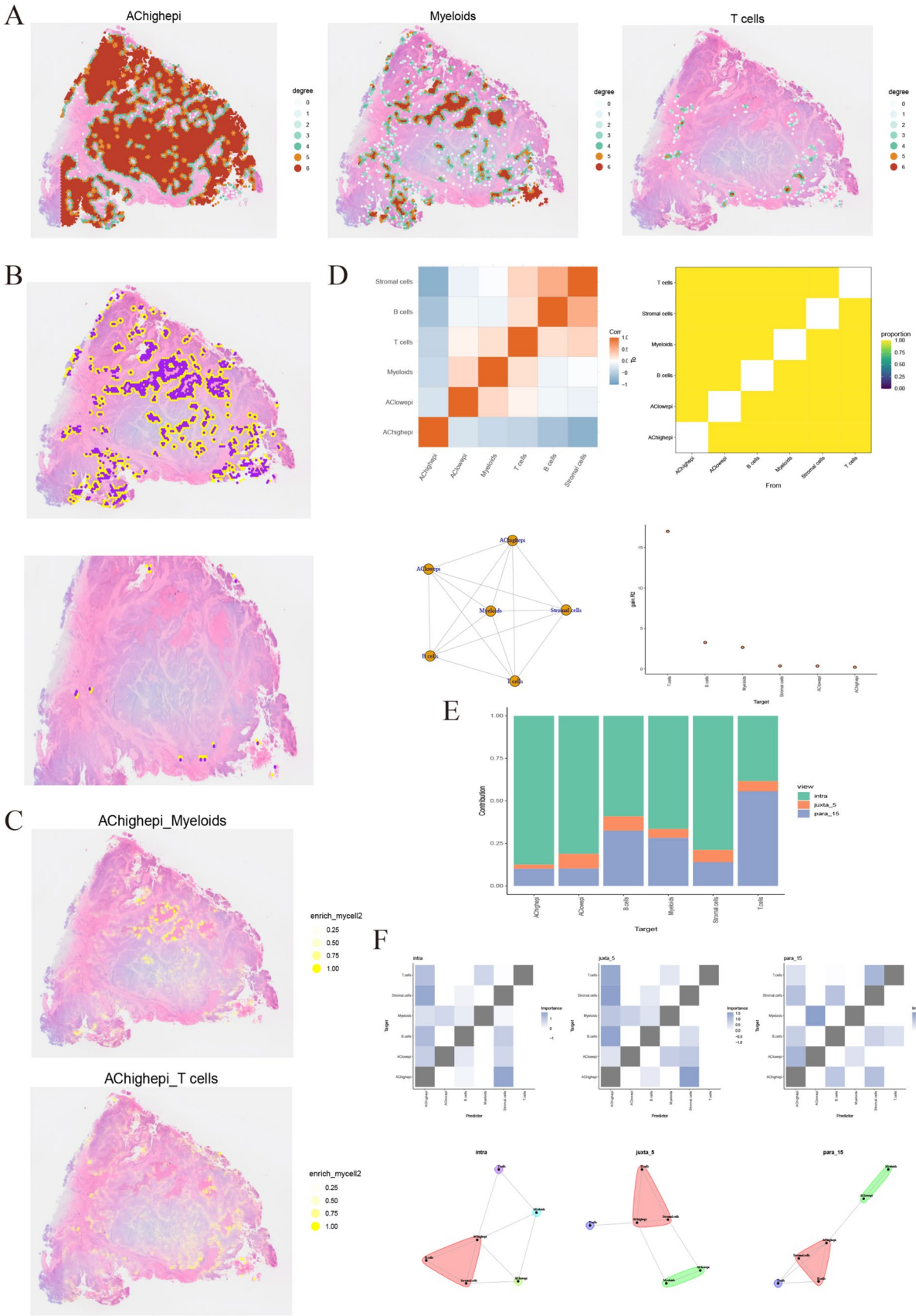
A
AChighepi
Myeloids
T cells
degree
B
C
AChighepi_Myeloids
AChighepi_T cells
enrich_mycell2
0.25
0.50
0.75
1.00
D
Stromal cells
B cells
T cells
Myeloids
AClowepi
AChighepi
proportion
From
E
Contribution
Target
view
intra
juxta_5
para_15
F
intra
juxta_5
para_15
Predictor
Importance

Fig. 4 Single-cell data analysis of the NAT10 gene. **A** UMAP visualization of tumor tissue in single-cell data, with cells divided into six types. ▶ **B** Expression of NAT10 in various cell types. **C** Scatter plot and density plot of gene expression intensity of NAT10 under UMAP visualization. **D** Cell communication map of NAT10-positive epithelial cells, with line thickness representing communication strength. **E** Heatmap of cell communication in NAT10-positive epithelial cells. **F** Receptor-ligand intensity map of signaling pathways between NAT10 high and low expressing epithelial cells, myeloid cells, and T cells. **G** Principal component analysis (PCA) plot of epithelial cells. **H** PCA plot of epithelial cells after Harmony integration. **I** UMAP visualization of dimensionality-reduced clustered epithelial single-cell data, with colors representing different cell clusters (13 clusters in total). **J** Expression of NAT10 gene in epithelial cells. **K** Density plot of NAT10 gene expression in epithelial cells. **L** Pseudotemporal analysis plot of epithelial cells

bar charts of the analysis showed that the intraview and paraview contributed more to the target (Fig. 3E). In the specific network structure, AChighepi demonstrated strong interactions with myeloid cells and T cells in the intra and juxta_5 views. However, in the para_15 view, AChighepi was absent in its communication with myeloid cells. (Fig. 3F).

3.4 Multi-omics analysis of NAT10 positive epithelial cells

Single-cell data from the tumor group were extracted, and after cell annotation, UMAP visualization was performed (Fig. 4A). NAT10 exhibited higher expression in epithelial cells (Fig. 4B). FeaturePlot was used to show the gene expression in the UMAP reduced space, observing the distribution of the gene across different cell populations, while Density was used to show the expression density of the gene in the spatial context. Both plots together revealed high expression of NAT10 in epithelial cells (Fig. 4C). Based on the differential expression of NAT10, epithelial cells were divided into positive and negative epithelial cells. The communication between positive epithelial cells and other cell populations varied, with stronger communication with myeloid cells and T cells (Fig. 4D). In epithelial cells, there was a significant difference in the communication intensity between NAT10-positive and negative epithelial cells with myeloid cells and T cells (Fig. 4E). For myeloid cells and the same receptor-ligand pairs, positive epithelial cells exhibited stronger expression intensity than negative epithelial cells and also had more receptor-ligand pathways (Fig. 4F).

After extracting the epithelial cells, principal component analysis (PCA) and elbow curve analysis were performed (Fig. 4G), followed by Harmony batch effect correction (Fig. 4H). We still chose PC = 10 for dimensionality reduction and clustering, which resulted in 13 clusters (Fig. 4I). Cluster 4 had stronger NAT10 expression (Fig. 4J), and the density of NAT10 gene expression varied across clusters (Fig. 4K). Subsequently, pseudotime analysis revealed that cell cluster 4, which had high NAT10 expression, served as the starting point for dynamic cell changes (Fig. 4L), providing evidence of its potential role in colon cancer tissues. This suggests that NAT10 may enhance the expression of other acetylation-related genes, which could explain why epithelial cells with high acetylation-gene expression appear as endpoints in the pseudotime trajectory analysis. This finding highlights the potential role of NAT10 in colon cancer tissue.

Spatial transcriptomics analysis was performed to assess tissue sections and NAT10 expression (Fig. 5A, B). After SCTransform and cpm normalization, cells were clustered into 17 groups (Fig. 5C), with NAT10 remaining highly expressed (Fig. 5D). Given the lower resolution of spatial transcriptomics compared to single-cell RNA sequencing, deconvolution analysis using RCTD was employed to evaluate cell proportions of NAT10 + epi, NAT-epi, myeloid cells, and T cells (Fig. 5E, F). Misty analysis further examined spatial relationships between cell types (Fig. 5G, H). Bar chart results revealed that intraview and paraview contributed most to cell interactions, with positive cells interacting with myeloid cells and T cells. Notably, in the paraview, communication between positive cells and myeloid cells was absent (Fig. 5I). These results align with the acetylation gene set analysis, reinforcing NAT10's role as a representative gene.

In the homotypic cell network, the communication intensity between cells is shown (Fig. 6A). In the heterotypic network, the interaction between NAT10 + epi and myeloid cells was stronger than with T cells (Fig. 6B, C). Enrichment analysis revealed that positive epithelial cells showed strong interactions with myeloid cells at certain locations in the tumor tissue, but their interaction with T cells spanned a wider range (Fig. 6D, E). This finding aligns with the Misty analysis results.

3.5 Multi-omics analysis of GNE positive epithelial cells

The same procedure was repeated, and GNE was also highly expressed in epithelial cells (Fig. 7A–C). Similar to the NAT10 gene, positive epithelial cells exhibited intense communication, with significant differences in interaction with myeloid cells and T cells compared to negative epithelial cells. The intensity of receptor-ligand pathways was also visualized (Fig. 7D–G). After extracting epithelial cells, we observed the expression level and density of GNE (Fig. 7H–J), followed

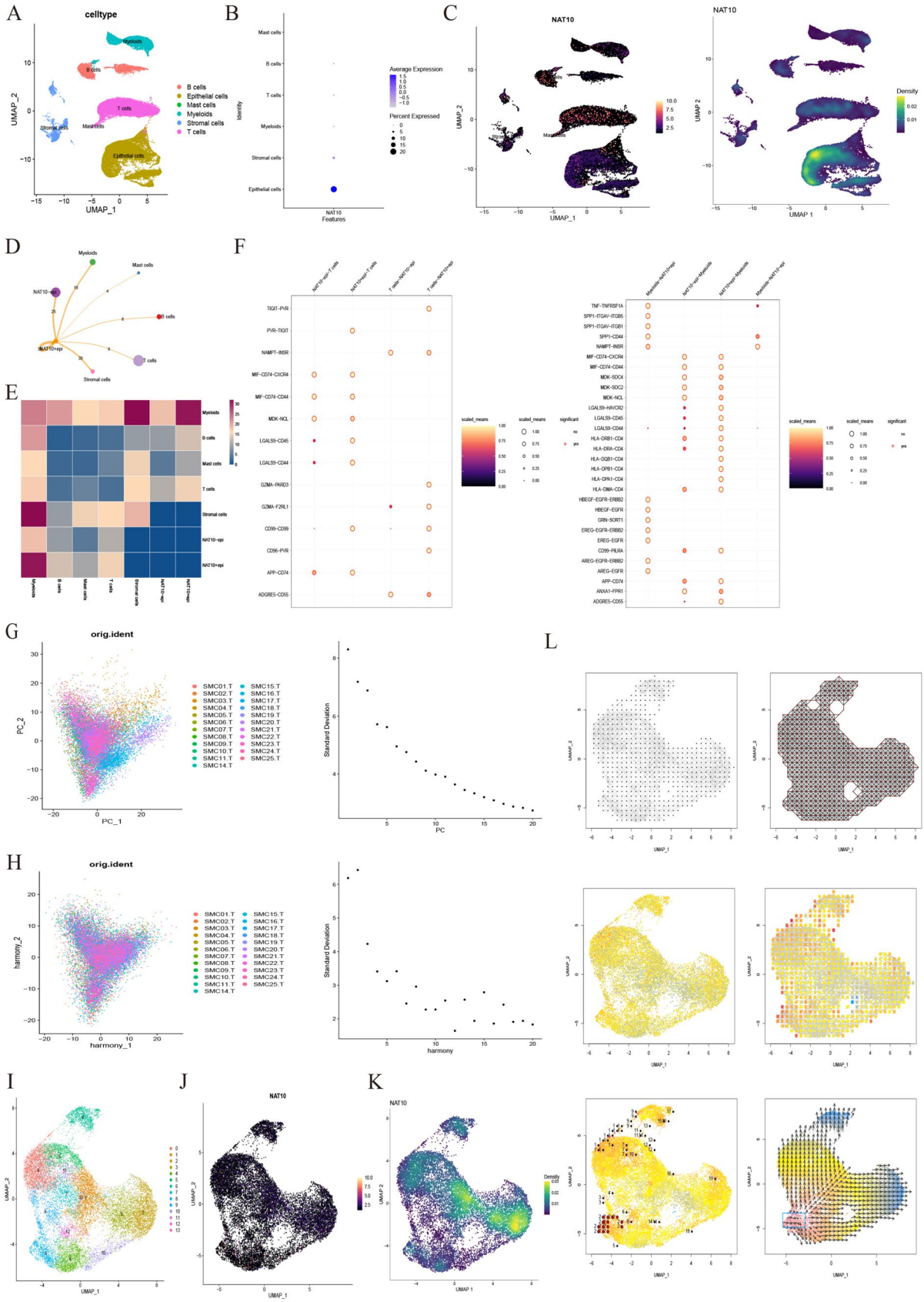
A
celltype
B cells
Epithelial cells
Mast cells
Myeloids
Stromal cells
T cells
UMAP_1
UMAP_2
B
Mast cells
B cells
T cells
Myeloids
Stromal cells
Epithelial cells
Identity
NAT10
Features
Average Expression
Percent Expressed
C
NAT10
UMAP_1
UMAP_2
NAT10
UMAP 1
UMAP 2
Density
D
Myeloids
Mast cells
NAT10−
B cells
NAT10+epi
T cells
Stromal cells
E
Myeloids
B cells
Mast cells
T cells
Stromal cells
NAT10−epi
NAT10+epi
F
NAT10−epi−T cells
NAT10+epi−T cells
T cells−NAT10−epi
T cells−NAT10+epi
TIGIT−PVR
PVR−TIGIT
NAMPT−INSR
MIF−CD74−CXCR4
MIF−CD74−CD44
MDK−NCL
LGALS9−CD45
LGALS9−CD44
GZMA−PARD3
GZMA−F2RL1
CD99−CD99
CD96−PVR
APP−CD74
ADGRE5−CD55
scaled_means
significant
Myeloids−NAT10+epi
NAT10−epi−Myeloids
NAT10+epi−Myeloids
Myeloids−NAT10−epi
TNF−TNFRSF1A
SPP1−ITGAV−ITGB5
SPP1−ITGAV−ITGB1
SPP1−CD44
NAMPT−INSR
MIF−CD74−CXCR4
MIF−CD74−CD44
MDK−SDC4
MDK−SDC2
MDK−NCL
LGALS9−HAVCR2
LGALS9−CD45
LGALS9−CD44
HLA−DRB1−CD4
HLA−DRA−CD4
HLA−DQB1−CD4
HLA−DPB1−CD4
HLA−DPA1−CD4
HLA−DMA−CD4
HBEGF−EGFR−ERBB2
HBEGF−EGFR
GRN−SORT1
EREG−EGFR−ERBB2
EREG−EGFR
CD99−PILRA
AREG−EGFR−ERBB2
AREG−EGFR
APP−CD74
ANXA1−FPR1
ADGRE5−CD55
G
orig.ident
PC_1
PC_2
SMC01.T
SMC02.T
SMC03.T
SMC04.T
SMC05.T
SMC06.T
SMC07.T
SMC08.T
SMC09.T
SMC10.T
SMC11.T
SMC14.T
SMC15.T
SMC16.T
SMC17.T
SMC18.T
SMC19.T
SMC20.T
SMC21.T
SMC22.T
SMC23.T
SMC24.T
SMC25.T
Standard Deviation
PC
L
UMAP_1
UMAP_2
H
orig.ident
harmony_1
harmony_2
Standard Deviation
harmony
I
J
NAT10
K
NAT10
UMAP_1
UMAP_2

Fig. 5 Spatial transcriptomics data of NAT10 expression. **A** H&E staining atlas of CC tumor tissue slices and quality control of spatial transcriptomics data. **B** Expression intensity of NAT10 in spatial transcriptomics. **C** UMAP visualization of dimensionality-reduced clustered spatial transcriptomics data, resulting in 17 cell clusters. **D** Expression of NAT10 after normalization. **E** Spatial distribution probability of NAT10-positive and negative epithelial cells after RCTD. **F** Spatial distribution probability of myeloid cells and T cells. **G** Correlation strength and population plot of each cell under MistyR package analysis. **H** Cell communication network plot and relative importance under MistyR package analysis. **I** Bar plot showing the contribution of three perspectives under MistyR package analysis. **J** Heatmap and network plot of cell communication under three different perspectives

by pseudotime analysis. In contrast to the previous acetylation-related gene set and NAT10 analysis, cell clusters 0 and 6 with high GNE expression did not serve as the starting points of the cell development trajectory (Fig. 7K).

After completing single-cell omics analysis, RCTD was performed. In the spatial plane of tissue slices, the proportion of positive epithelial cells was lower than that of negative epithelial cells (Fig. 7L). The discrepancies in both analyses may suggest that GNE may not be the key gene in acetylation that drives the increased risk of colon cancer. In MistyR, intraview and paraview again contributed the most (Fig. 7M). Interestingly, in the paraview, myeloid cells and GNE-positive epithelial cells were clustered together, revealing their potential shared biological functions (Fig. 7N).

Subsequent CellDegree analysis showed that both homotypic and heterotypic networks had much lower interaction intensity compared to NAT10 (Fig. 7O–Q), and enrichment analysis yielded similar results (Fig. 7R, S).

3.6 Prognosis and immune therapy of positive epithelial cells

Through multi-omics analysis, we found that the three types of positive epithelial cells play important roles in colon cancer, with NAT10 and GNE identified as key genes. Survival analysis of key gene-positive epithelial cells in colon cancer samples from the TCGA database showed that GNE-positive epithelial cells had a higher survival rate compared to the normal group ($p = 0.015$), which was contrary to the results from the SMR analysis (Fig. 8A). On the other hand, NAT10-positive epithelial cells showed poorer prognosis ($p = 0.012$), acting as a risk factor, which was consistent with the SMR results (Fig. 8B), suggesting that NAT10 promotes the growth and metastasis of primary colon cancer. Given that NAT10-positive epithelial cells show strong interaction with myeloid cells and T cells, we further analyzed the immune escape mechanism using the TIDE algorithm. In NAT10-positive epithelial cells, there were more non-responsive individuals to immune checkpoint blockade therapy (Fig. 8C), showing a statistically significant difference ($p = 1.3e{-}5$). Additionally, the MSI score was negatively correlated with NAT10-positive epithelial cells (r_Pearson = −0.14, $p = 1.90e{-}3$), indicating poor sensitivity to ICB therapy (Fig. 8D).

In the TIDE algorithm, immune suppressor cells include MDSCs within myeloid cells. A positive correlation was observed between positive epithelial cells and MDSCs (r_Pearson = 0.47, $p = 4.39e{-}27$), suggesting that positive epithelial cells promote MDSC proliferation, facilitating tumor immune escape (Fig. 8E).For T cells, CD8 expression showed a slight but non-significant increase with more NAT10-positive epithelial cells (r_Pearson = 0.01, $p = 0.80$, Fig. 8F). However, CD274 (PD-L1) expression significantly decreased (r_Pearson = −0.19, $p = 2.59e{-}5$), potentially impairing CTL-mediated tumor cell killing and aiding immune evasion (Fig. 8G). Additionally, high positive epithelial cell expression correlated with increased T cell clearance in tumor patients (r_Pearson = 0.29, $p = 7.5e{-}11$), impacting cellular immunity (Fig. 8H). These findings indicate that NAT10-positive epithelial cells promote colon cancer growth and metastasis, acting as a significant risk factor.

4 Discussion

NAT10 (*N*-acetyltransferase 10) is a key RNA acetyltransferase, and recent studies have shown that it plays a critical role in the occurrence, development, and metastasis of various cancers [32–34]. In hepatocellular carcinoma (HCC), overexpression of NAT10 is closely related to the stability of mutant p53. NAT10 inhibits the function of Mdm2 through deacetylation, enhancing the stability of mutant p53 and promoting its oncogenic effects. This mechanism suggests that NAT10 not only plays a significant role in regulating RNA translation but also contributes to cancer initiation and progression by regulating the stability of key tumor suppressors [35]. In head and neck squamous cell carcinoma (HNSCC), NAT10 overexpression promotes the activation of signaling pathways such as MYC, E2F, and mTORC1, thereby enhancing cancer cell proliferation, migration, and invasion abilities. Moreover, inhibiting NAT10 expression via gene silencing or small molecule inhibitors significantly weakens these malignant features of cancer cells, further validating its potential as a therapeutic target [36]. Interestingly, some studies have found that NAT10 catalyzes the N4-acetylcytidine

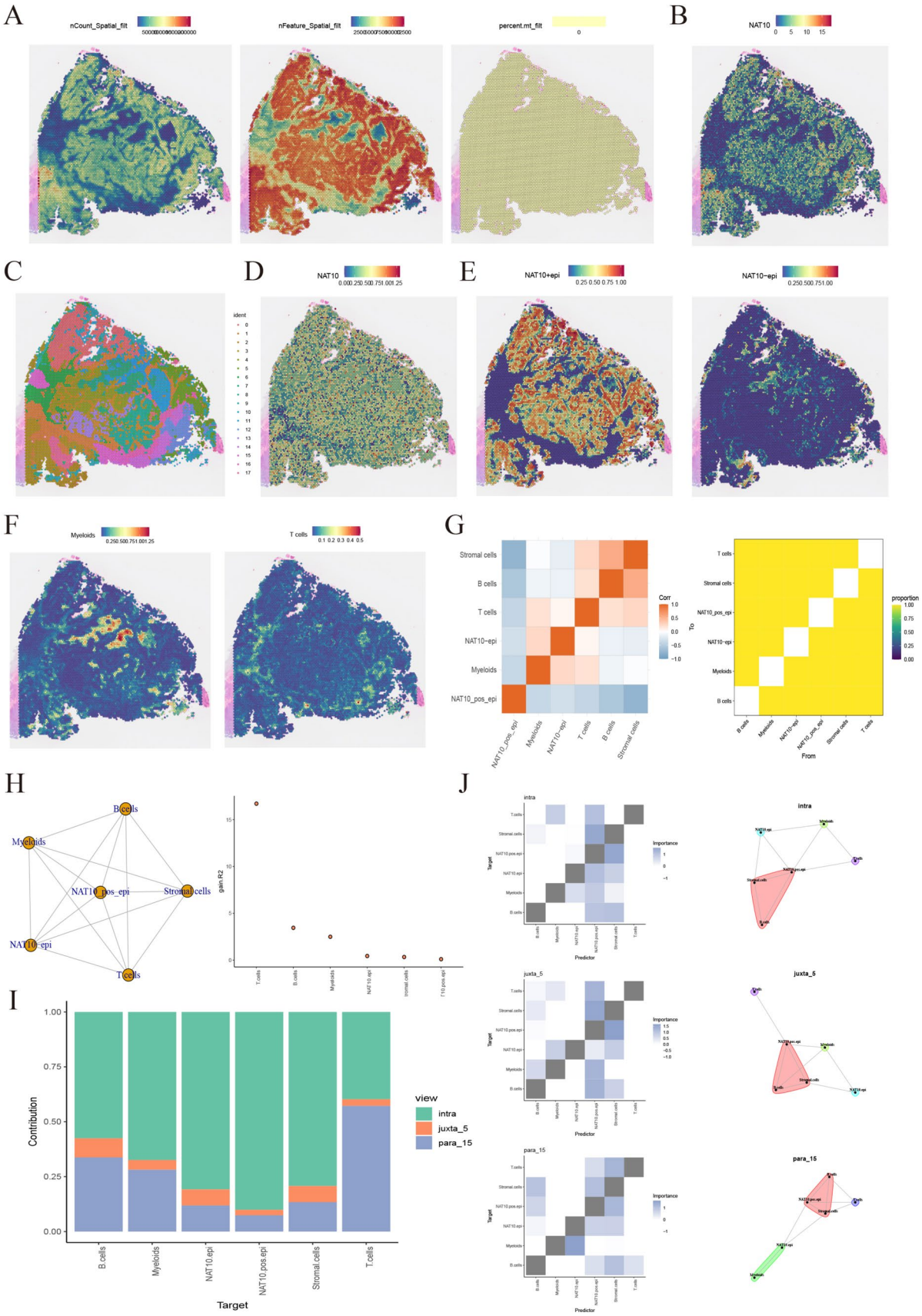
A
nCount_Spatial_filt
nFeature_Spatial_filt
percent.mt_filt
B
NAT10
C
D
NAT10
E
NAT10+epi
NAT10−epi
F
Myeloids
T cells
G
Stromal cells
B cells
T cells
NAT10−epi
Myeloids
NAT10_pos_epi
Corr
To
From
proportion
H
B cells
Myeloids
NAT10_pos_epi
Stromal cells
NAT10−epi
T cells
gain.R2
J
intra
juxta_5
para_15
Importance
Target
Predictor
I
Contribution
Target
B.cells
Myeloids
NAT10.epi
NAT10.pos.epi
Stromal.cells
T.cells
view
intra
juxta_5
para_15

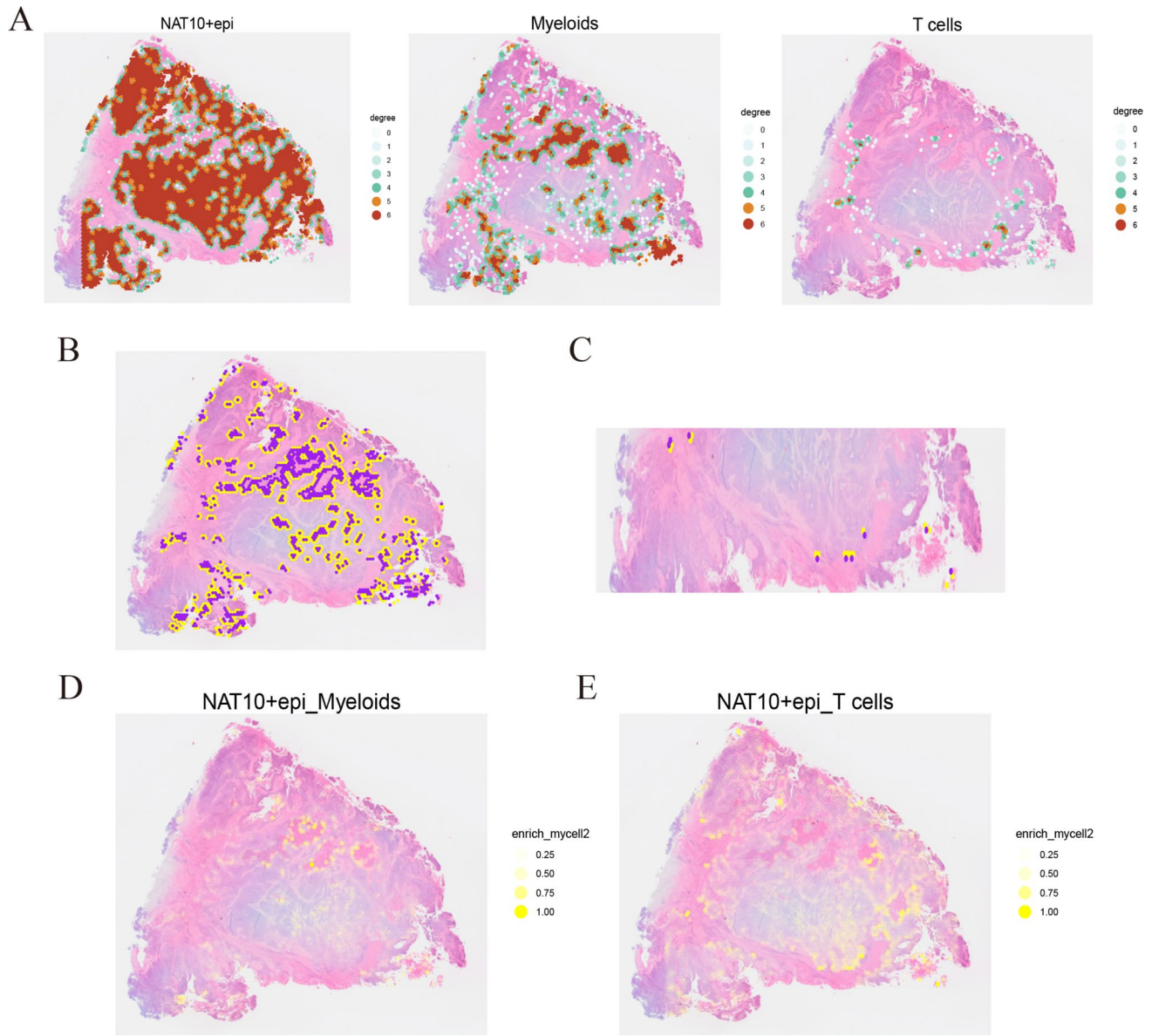

Fig. 6 Cell communication differences between NAT10-positive epithelial cells and myeloid cells and T cells based on CellDegree analysis. **A** Homotypic cell network plot. **B** Heterotypic cell network plot of NAT10-positive epithelial cells and myeloid cells. **C** Heterotypic cell network plot of NAT10-positive epithelial cells and T cells. **D** Neighboring cell enrichment analysis plot of NAT10-positive epithelial cells and myeloid cells. **E** Neighboring cell enrichment analysis plot of NAT10-positive epithelial cells and T cells

(ac4C) modification on mRNA, significantly regulating mRNA stability and translation efficiency, and contributing to the chemoresistance of colon cancer stem cells [37]. NAT10 can also inhibit ferroptosis in colon cancer cells, promoting tumor growth and metastasis [38]. These findings align with our bioinformatics analysis results, suggesting that NAT10 could be a risk factor for colon cancer.

This study used multi-omics analysis to investigate the role of acetylation-related genes in colon cancer, identifying key genes like NAT10 and GNE. These genes are involved in cancer initiation, growth, metastasis, and immune evasion. The research highlights the importance of acetylation in colon cancer and identifies NAT10 as a potential target for early diagnosis and therapy. Additionally, NAT10-positive epithelial cells are linked to poor prognosis by promoting immune evasion.

Although this study has yielded important findings, it still has some limitations. First, there are limitations in the bioinformatics analysis methods. The resolution of spatial transcriptomics data is relatively low compared to single-cell RNA sequencing, leading to discrepancies in the precision of cell type localization analysis. While we used deconvolution analysis to mitigate this limitation, the differences between the two technologies may still cause biases in the interpretation of cell population distributions. Second, there is a lack of experimental validation. Although multi-omics analysis provides strong evidence for the correlation between acetylation genes and colon cancer, these findings are primarily based on data correlation analyses and lack further experimental validation, particularly in vivo experiments to confirm the direct causal relationship between NAT10-positive epithelial cells and tumor initiation.

While previous experiments have explored the relationship between NAT10 and colon cancer, our analysis reveals that NAT10-positive epithelial cells show strong interactions with myeloid cells, T cells, and, notably, immune-suppressive cells (such as MDSCs). However, there is a lack of in vivo and in vitro experiments specifically focusing on the interaction between NAT10-positive epithelial cells and immune cells. This research direction holds great promise and is of significant importance for the treatment of primary colon cancer.

5 Conclusions

This study underscores the crucial role of acetylation-related genes, particularly NAT10 and GNE, in the progression of colon cancer. By employing a multi-omics approach that integrates SMR, single-cell RNA sequencing, spatial transcriptomics, and deconvolution analysis through RCTD, we gained valuable insights into the spatial and cellular dynamics of colon cancer. Our findings highlight the significant interactions between NAT10-positive epithelial cells and both myeloid cells and T cells, offering critical understanding of the immune evasion mechanisms within the tumor microenvironment. Additionally, analysis of cell communication networks using tools such as MistyR and CellDegree further illuminated the complex relationships between these cell populations. Crucially, our study reveals that NAT10-positive epithelial cells are linked to poorer prognosis in colon cancer, suggesting their potential as therapeutic targets. These cells not only play a central role in the tumor microenvironment but also contribute to immune escape, reducing the effectiveness of immune checkpoint blockade therapies. While these insights are promising, the study acknowledges certain limitations, such as the relatively low resolution of spatial transcriptomics data and the absence of experimental validation. Future research should focus on in vivo and in vitro studies to validate these associations and explore the therapeutic potential of targeting NAT10 in colon cancer.

Fig. 7 Multi-omics data analysis of GNE gene expression. **A** Bubble plot of GNE expression intensity across various cell types. **B** Distribution of GNE gene expression under UMAP visualization. **C** Density plot of GNE gene expression. **D** Heatmap of communication differences between GNE and various cell types. **E** Cell communication map of GNE-positive epithelial cells, with line thickness representing communication strength. **F** Receptor-ligand intensity map of signaling pathways between GNE-positive epithelial cells, acetylation-negative epithelial cells, and myeloid cells. **G** Receptor-ligand intensity map of signaling pathways between GNE-positive epithelial cells, acetylation-negative epithelial cells, and T cells. **H** UMAP visualization of dimensionality-reduced clustered single-cell epithelial data, with colors representing different cell clusters (13 clusters in total). **I** Expression of GNE gene in epithelial cells. **J** Density plot of GNE gene expression in epithelial cells. **K** Pseudotemporal analysis plot of epithelial cells. **L** Spatial distribution probability of GNE-positive and GNE-negative epithelial cells. **M** Bar plot showing the contribution of different views to the cell interaction evaluation by the MistyR package, highlighting the relative importance of each. **N** Communication strength and interaction networks of cells under three different perspectives. **O** Communication strength of GNE-positive epithelial cells in the homotypic cell network. **P** Heterotypic cell network plot of GNE-positive epithelial cells and myeloid cells. **Q** Heterotypic cell network plot of GNE-positive epithelial cells and T cells. **R** Neighboring cell enrichment analysis plot of GNE-positive epithelial cells and myeloid cells. **S** Neighboring cell enrichment analysis plot of GNE-positive epithelial cells and T cells

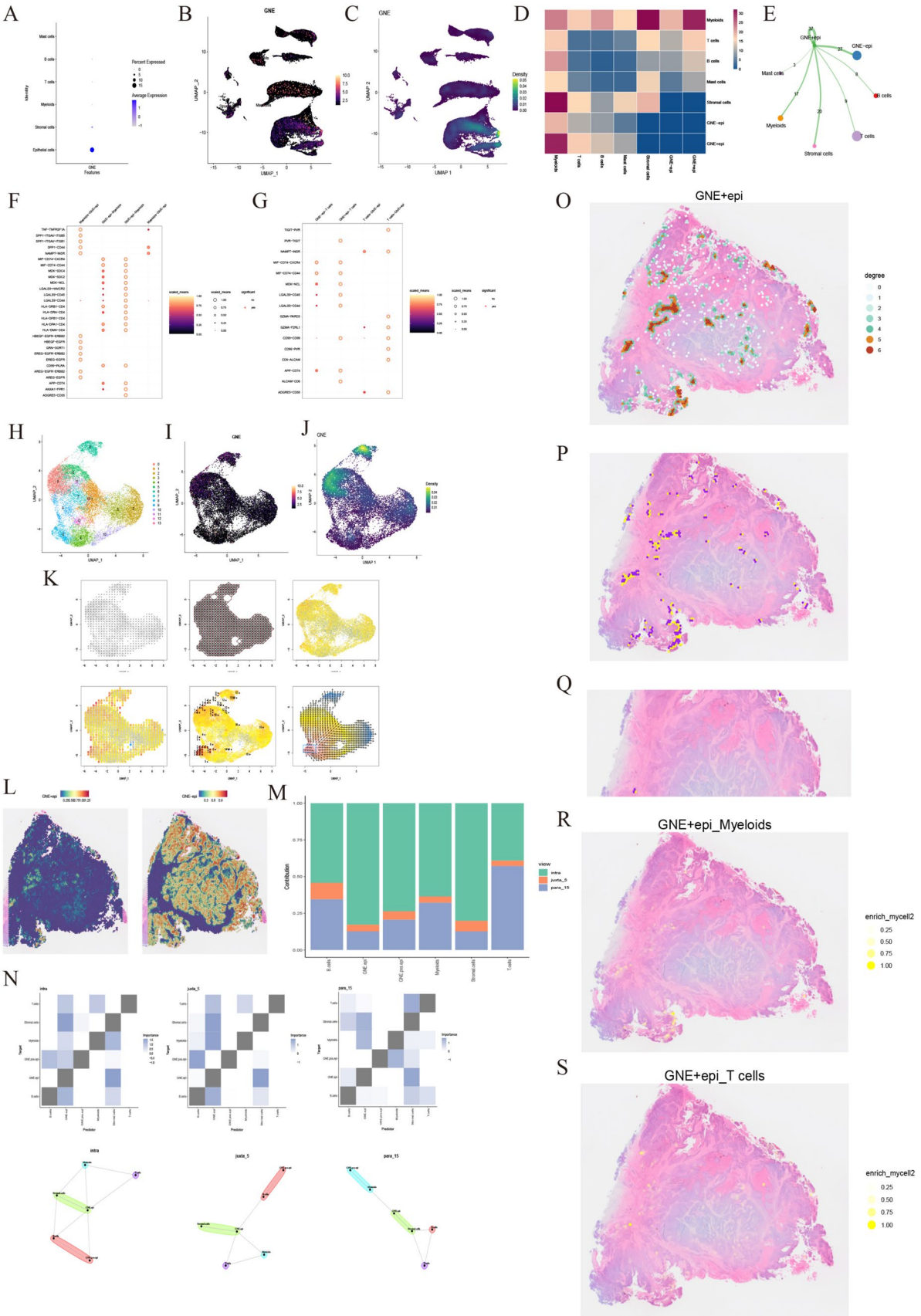
A
B
GNE
C
GNE
D
E
F
G
O
GNE+epi
degree
H
I
GNE
J
GNE
P
K
Q
L
M
Contribution
view
intra
juxta_5
para_15
R
GNE+epi_Myeloids
enrich_mycell2
N
S
GNE+epi_T cells
enrich_mycell2

Fig. 8 Clinical prognostic value of acetylation genes NAT10 and GNE. **A** Kaplan–Meier (K–M) curve for overall survival of colon cancer patients, with patients divided into high-expression and low-expression groups based on GNE-positive epithelial cell marker genes. **B** Kaplan–Meier (K–M) curve for overall survival of colon cancer patients, with patients divided into high-expression and low-expression groups based on NAT10-positive epithelial cell marker genes. **C** Box plot of TIDE immune therapy response. **D**–**H** Correlation between NAT10-positive epithelial cells and immune-related marker genes

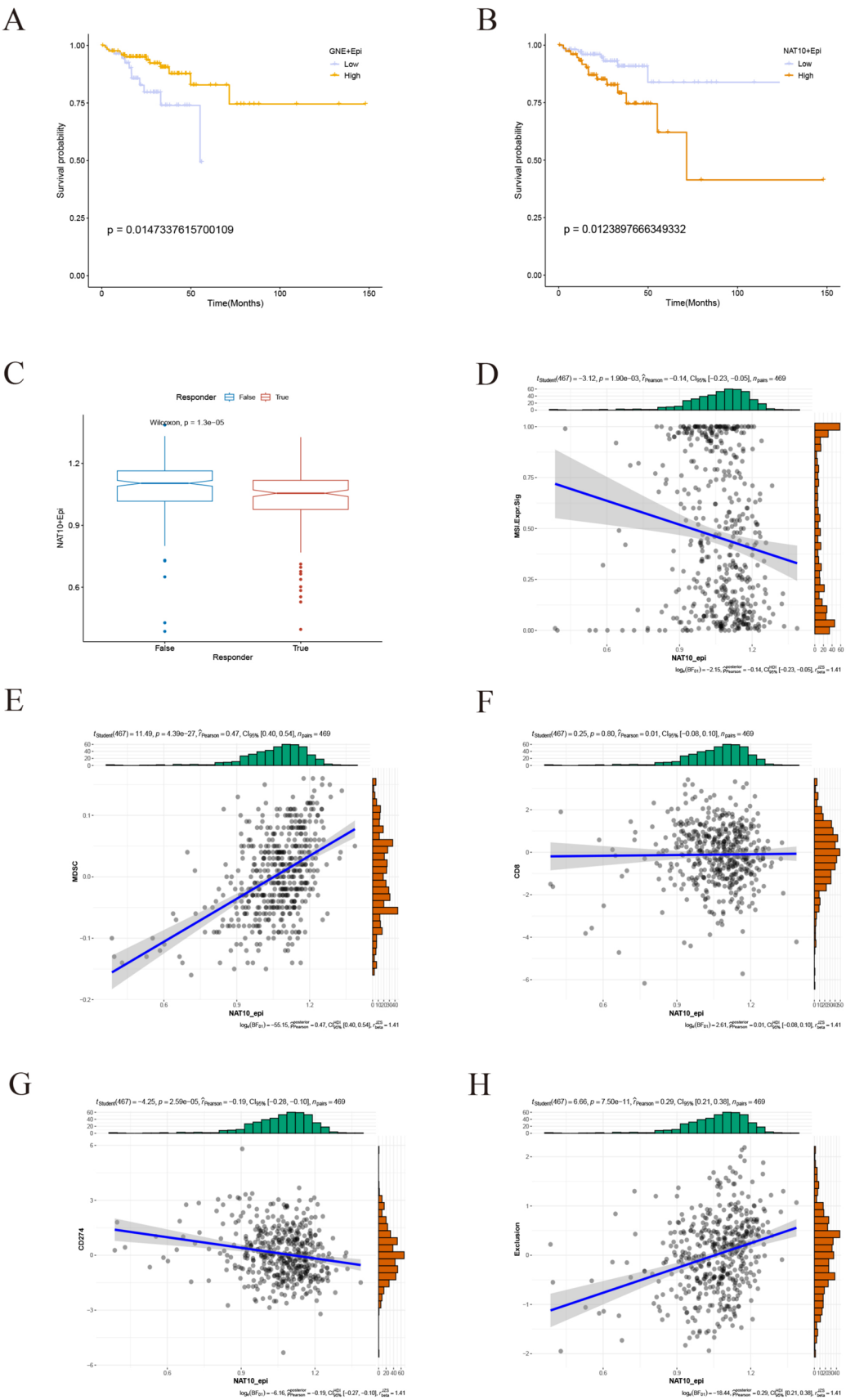
A
GNE+Epi
Low
High
Survival probability
p = 0.0147337615700109
Time(Months)
B
NAT10+Epi
Low
High
Survival probability
p = 0.0123897666349332
Time(Months)
C
Responder False True
Wilcoxon, p = 1.3e−05
NAT10+Epi
False
True
Responder
D
MSI.Expr.Sig
NAT10_epi
E
MDSC
NAT10_epi
F
CD8
NAT10_epi
G
CD274
NAT10_epi
H
Exclusion
NAT10_epi

Author contributions XCZ, XS, LJ, SKZ, and CLJ collected the data. YHG, GHY, JYZ, and YPF wrote the manuscript and analyzed the data. HC, XCZ, XS, BBW, and XLZ designed the research study. All authors approved the final version of the manuscript.

Funding Sichuan Medical Science and Technology Innovation Research Association (hereinafter referred to as Sichuan Medical Innovation Association) launched the special scientific research project of "Top of Medical Innovation". 2025.01–2027.03, Project Leader, 200,000 RMB. Project Approval Code: YCH-KY-YCZD2024-298.

Data availability All original data for this paper was obtained from TCGA and GEO public databases and all original data and documents can be found.

Declarations

Conflict of interests The authors declare no competing interests.

References

1. Riihimäki M, Hemminki A, Sundquist J, Hemminki K. Patterns of metastasis in colon and rectal cancer. Sci Rep. 2016;6:29765.
2. Yang Z, Chen Y, Wu D, Min Z, Quan Y. Analysis of risk factors for colon cancer progression. Onco Targets Ther. 2019;12:3991–4000.
3. Jacobs D, Zhu R, Luo J, Grisotti G, Heller DR, Kurbatov V, Johnson CH, Zhang Y, Khan SA. Defining early-onset colon and rectal cancers. Front Oncol. 2018;8:504.
4. Paschke S, Jafarov S, Staib L, Kreuser ED, Maulbecker-Armstrong C, Roitman M, Holm T, Harris CC, Link KH, Kornmann M. Are colon and rectal cancer two different tumor entities? A proposal to abandon the term colorectal cancer. Int J Mol Sci. 2018;19:2577.
5. Asghari-Jafarabadi M, Wilkins S, Plazzer JP, Yap R, McMurrick PJ. Prognostic factors and survival disparities in right-sided versus left-sided colon cancer. Sci Rep. 2024;14:12306.
6. Han S, Wang D, Huang Y, Zeng Z, Xu P, Xiong H, Ke Z, Zhang Y, Hu Y, Wang F, Wang J, Zhao Y, Zhuo W, Zhao G. A reciprocal feedback between colon cancer cells and Schwann cells promotes the proliferation and metastasis of colon cancer. J Exp Clin Cancer Res. 2022;41:348.
7. Pacal I, Karaboga D, Basturk A, Akay B, Nalbantoglu U. A comprehensive review of deep learning in colon cancer. Comput Biol Med. 2020;126: 104003.
8. Ding P, Ma Z, Liu D, Pan M, Li H, Feng Y, Zhang Y, Shao C, Jiang M, Lu D, Han J, Wang J, Yan X. Lysine acetylation/deacetylation modification of immune-related molecules in cancer immunotherapy. Front Immunol. 2022;13: 865975.
9. Wang C, Ma X. The role of acetylation and deacetylation in cancer metabolism. Clin Transl Med. 2025;15: e70145.
10. Xia C, Tao Y, Li M, Che T, Qu J. Protein acetylation and deacetylation: an important regulatory modification in gene transcription (review). Exp Ther Med. 2020;20:2923–40.
11. Sun X, Shu Y, Ye G, Wu C, Xu M, Gao R, Huang D, Zhang J. Histone deacetylase inhibitors inhibit cervical cancer growth through Parkin acetylation-mediated mitophagy. Acta Pharm Sin B. 2022;12:838–52.
12. Minic Z, Li Y, Hüttmann N, Uppal GK, D'Mello R, Berezovski MV. Lysine acetylome of breast cancer-derived small extracellular vesicles reveals specific acetylation patterns for metabolic enzymes. Biomedicines. 2023;11:1076.
13. Wang X, Li N, Zheng M, Yu Y, Zhang S. Acetylation and deacetylation of histone in adipocyte differentiation and the potential significance in cancer. Transl Oncol. 2024;39: 101815.
14. Narayan S, Bader GD, Reimand J. Frequent mutations in acetylation and ubiquitination sites suggest novel driver mechanisms of cancer. Genome Med. 2016;8:55.
15. Liu C, Yang Q, Zhu Q, Lu X, Li M, Hou T, Li Z, Tang M, Li Y, Wang H, Yang Y, Wang H, Zhao Y, Wen H, Liu X, Mao Z, Zhu WG. CBP mediated DOT1L acetylation confers DOT1L stability and promotes cancer metastasis. Theranostics. 2020;10:1758–76.
16. Deng Y, Gao J, Xu G, Yao Y, Sun Y, Shi Y, Hao X, Niu L, Li H. HDAC6-dependent deacetylation of AKAP12 dictates its ubiquitination and promotes colon cancer metastasis. Cancer Lett. 2022;549: 215911.
17. Hong YJ, Park J, Hahm JY, Kim SH, Lee DH, Park KS, Seo SB. Regulation of UHRF1 acetylation by TIP60 is important for colon cancer cell proliferation. Genes Genomics. 2022;44:1353–61.
18. Wang W, Liu Y, Wang Z, Tan X, Jian X, Zhang Z. Exploring and validating the necroptotic gene regulation and related lncRNA mechanisms in colon adenocarcinoma based on multi-dimensional data. Sci Rep. 2024;14:22251.
19. Wehby GL, Ohsfeldt RL, Murray JC. 'Mendelian randomization' equals instrumental variable analysis with genetic instruments. Stat Med. 2008;27:2745–9.
20. Zhu T, Gao P, Ma Y, Yang P, Cao Z, Gao J, Du J, Jiang H, Zhang X. Mitochondrial FIS1 as a novel drug target for the treatment of erectile dysfunction: a multi-omic and epigenomic association study. World J Mens Health. 2024;42: e93.

21. Xie J, Ma R, Xu X, Yang M, Yu H, Wan X, Xu K, Guo J, Xu P. Identification of genetic association between mitochondrial dysfunction and knee osteoarthritis through integrating multi-omics: a summary data-based Mendelian randomization study. Clin Rheumatol. 2024;43:3487–96.
22. Lin W, Wang J, Ge J, Zhou R, Hu Y, Xiao L, Peng Q, Zheng Z. The activity of cuproptosis pathway calculated by AUCell algorithm was employed to construct cuproptosis landscape in lung adenocarcinoma. Discov Oncol. 2023;14:135.
23. Andreatta M, Carmona SJ. UCell: robust and scalable single-cell gene signature scoring. Comput Struct Biotechnol J. 2021;19:3796–8.
24. Hänzelmann S, Castelo R, Guinney J. GSVA: gene set variation analysis for microarray and RNA-seq data. BMC Bioinformatics. 2013;14:7.
25. Jin S, Plikus MV, Nie Q. Cell Chat for systematic analysis of cell-cell communication from single-cell transcriptomics. Nat Protoc. 2025;20:180–219.
26. Cheng J, Xiao M, Meng Q, Zhang M, Zhang D, Liu L, Jin Q, Fu Z, Li Y, Chen X, Xie H. Decoding temporal heterogeneity in NSCLC through machine learning and prognostic model construction. World J Surg Oncol. 2024;22:156.
27. Cable DM, Murray E, Zou LS, Goeva A, Macosko EZ, Chen F, Irizarry RA. Robust decomposition of cell type mixtures in spatial transcriptomics. Nat Biotechnol. 2022;40:517–26.
28. Tanevski J, Flores ROR, Gabor A, Schapiro D, Saez-Rodriguez J. Explainable multiview framework for dissecting spatial relationships from highly multiplexed data. Genome Biol. 2022;23:97.
29. Zheng Y, Carrillo-Perez F, Pizurica M, Heiland DH, Gevaert O. Spatial cellular architecture predicts prognosis in glioblastoma. Nat Commun. 2023;14:4122.
30. Shi J, Bao M, Wang W, Wu X, Li Y, Zhao C, Liu W. Integrated profiling identifies PLOD3 as a potential prognostic and immunotherapy relevant biomarker in colorectal cancer. Front Immunol. 2021;12: 722807.
31. Xu S, Tang L, Liu Z, Luo C, Cheng Q. Hypoxia-related lncRNA correlates with prognosis and immune microenvironment in lower-grade glioma. Front Immunol. 2021;12: 731048.
32. Zou Y, Guo S, Wen L, Lv D, Tu J, Liao Y, Chen W, Chen Z, Li H, Chen J, Shen J, Xie X. Targeting NAT10 inhibits osteosarcoma progression via ATF4/ASNS-mediated asparagine biosynthesis. Cell Rep Med. 2024;5: 101728.
33. Jean MJ, Power D, Kong W, Huang H, Santoso N, Zhu J. Identification of HIV-1 Tat-associated proteins contributing to HIV-1 transcription and latency. Viruses. 2017;9:67.
34. Cao Y, Yao M, Wu Y, Ma N, Liu H, Zhang B. *N*-acetyltransferase 10 promotes micronuclei formation to activate the senescence-associated secretory phenotype machinery in colorectal cancer cells. Transl Oncol. 2020;13: 100783.
35. Li Q, Liu X, Jin K, Lu M, Zhang C, Du X, Xing B. NAT10 is upregulated in hepatocellular carcinoma and enhances mutant p53 activity. BMC Cancer. 2017;17:605.
36. Tao W, Tian G, Xu S, Li J, Zhang Z, Li J. NAT10 as a potential prognostic biomarker and therapeutic target for HNSCC. Cancer Cell Int. 2021;21:413.
37. Gao LP, Li TD, Yang SZ, Ma HM, Wang X, Zhang DK. NAT10-mediated ac^4C modification promotes stemness and chemoresistance of colon cancer by stabilizing NANOGP8. Heliyon. 2024;10: e30330.
38. Zheng X, Wang Q, Zhou Y, Zhang D, Geng Y, Hu W, Wu C, Shi Y, Jiang J. *N*-acetyltransferase 10 promotes colon cancer progression by inhibiting ferroptosis through N^4-acetylation and stabilization of ferroptosis suppressor protein 1 (FSP1) mRNA. Cancer Commun. 2022;42:1347–66.